J Biomol NMR (2011) 51:151–162
DOI 10.1007/s10858-011-9549-6

ARTICLE

Measurement of amide hydrogen exchange rates with the use of radiation damping

Jing-Song Fan · Jackwee Lim · Binhan Yu · Daiwen Yang

Received: 10 May 2011 / Accepted: 7 July 2011

Abstract A simple method for measuring amide hydrogen exchange rates is presented, which is based on the selective inversion of water magnetization with the use of radiation damping. Simulations show that accurate exchange rates can be measured despite the complications of radiation damping and cross relaxation to the exchange process between amide and water protons. This method cannot eliminate the contributions of the exchange-relayed NOE and direct NOE to the measured exchange rates, but minimize the direct NOE contribution. In addition, the amides with a significant amount of such indirect contributions are possible to be identified from the shape of the exchange peak intensity profiles or/and from the apparent relaxation rates of amide protons which are extracted from fitting the intensity profiles to an equation established here for our experiment. The method was tested on ubiquitin and also applied to an acyl carrier protein. The amide exchange rates for the acyl carrier protein at two pHs indicate that the entire protein is highly dynamic on the second timescale. Low protection factors for the residues in the regular secondary structural elements also suggest the presence of invisible unfolded species. The highly dynamic nature of the acyl carrier protein may be crucial for its interactions with its substrate and enzymes.

Keywords Amide hydrogen exchange · Protein dynamics · Protein structure · Conformational change · Radiation damping

Electronic supplementary material The online version of this article (doi:10.1007/s10858-011-9549-6) contains supplementary material, which is available to authorized users.

J.-S. Fan · J. Lim · B. Yu · D. Yang (✉)
Department of Biological Sciences, National University of Singapore, 14 Science Drive 4, Singapore 117543, Singapore
e-mail: dbsydw@nus.edu.sg

Introduction

Labile hydrogen atoms play important roles in the stability of biomolecules. Their exchange rates with water are associated with their accessibility to solvent, local and global dynamics, and hydrogen bond strength if they are involved in hydrogen bonding (Englander and Kallenbach 1983). In addition, the exchange rates are affected by external factors such as pH and salt concentration (Christoffersen et al. 1996). The information in exchange rates of amide protons with solvent protons can provide insights into structural and dynamic properties of a protein and may reveal unfolding events and protein–ligand and protein–protein interactions (Paterson et al. 1990).

A number of NMR-based methods have been developed for the measurement of amide hydrogen exchange (HX) rates with solvent. The most widely used approach is hydrogen–deuterium (H–D) exchange (Wagner and Wüthrich 1982), which can be employed to quantify HX rates smaller than 0.01 s^{-1}. This approach is suitable for the identification of amides involved in stable hydrogen bonding. Another frequently used approach is based on the exchange spectroscopy (EXSY) using homonuclear (Dobson et al. 1986; Otting et al. 1991) or heteronuclear experiments (Spera et al. 1991; Grzesiek and Bax 1993; Gemmecker et al. 1993; Mori et al. 1994; Hwang et al. 1997), which provides quite accurate measurement of HX rates in a range of 1–100 s^{-1}. In principle, the EXSY-based methods can be applied to the study of relatively slow exchanging amide protons with HX rates smaller than 1 s^{-1}. The third method relies on ^{15}N instead of ^{1}H to measure HX rates, which is suitable for HX rates in a range of $\sim$0.2–20 s^{-1} (Chevelkov et al. 2010). Although this method is free from the complication from water and cross-relaxation, its low experimental sensitivity limits its

application mainly to small proteins and unfolded proteins. Very fast exchanging amide protons with HX rates > 100 s^{-1} are often invisible in 2D HSQC and HMQC spectra and thus cannot be studied by the 2D-based methods.

In the implementation of the EXSY-based methods, elimination of false signals from NOEs between amide protons and their proximal protons is necessary. The first strategy is to selectively excite only the water protons and then transfer water magnetization to amide protons via an NOE mixing method (Grzesiek and Bax 1993; Gemmecker et al. 1993; Mori et al. 1994, 1996a, b; Hwang et al. 1997; Fitzkee et al. 2011). This strategy is often combined with the use of multiple measurements at different pH to differentiate NOE contributions from pure HX exchange effects (Mori et al. 1997; Fitzkee et al. 2011). For ^{13}C,^{15}N-labeled proteins, the selection is achieved using an INEPT filter to eliminate H_α signals that are excited by selective water proton pulses (Grzesiek and Bax 1993). For ^{15}N-labeled proteins, the selection can be achieved using a spin-echo filter to suppress H_α signals since they decay much faster than water signal, but the loss of water proton magnetization can be significant during the filter period (Mori et al. 1996b). The second strategy is to use an NOE-ROE mixing scheme instead of an NOE mixing scheme, which does not aim to achieve high selectivity in excitation (Hwang et al. 1997, 1998). This strategy suppresses most intra-molecular NOE peaks and exchange-relayed NOE peaks and measures the exchange rates without much contamination from cross-relaxation. However, this method is limited to the measurement of HX rates > 1 s^{-1}, especially for medium-sized proteins because amide proton magnetization decays much faster during the NOE-ROE mixing period than during the NOE (or EXSY) mixing period. In addition, the NOE-ROE mixing scheme may fail to suppress the NOE effects for unfolded proteins (Fitzkee et al. 2011). The third strategy is to select water proton magnetization using the radiation damping effect (Liepinsh and Otting 1995; Bockmann et al. 1996). At high magnetic fields, when water magnetization is inverted together with other protons, it returns back to the equilibrium state in tens of milliseconds due to the radiation damping effect (Mao and Ye 1997; Chen et al. 2000), but protons resonating at frequencies different from water remain in the inverted state. Using the radiation damping method, although only magnetization at the water frequency is aligned in an opposite direction with respect to other proton magnetizations, it seems difficult to quantify HX rates because analysis of the exchange process during the water recovery period is not straightforward.

Here we present an approach to quantify HX rates using the radiation damping method. Numerical simulations show that HX rates can be measured accurately albeit cross relaxation among protons being significant in macromolecules, and radiation damping and amide-water exchange occurring simultaneously. Simulations also indicate that discrimination of the direct NOE and exchange-relayed NOE effects from the pure exchange effect is possible from the measured apparent relaxation rates of amide protons. The approach is demonstrated on ubiquitin and then applied to an acyl carrier protein (ACP).

Theory

All protons in a protein are coupled to one another in terms of dipole–dipole interactions. To analyze the evolution of an amide proton magnetization accurately, it is necessary to consider all protons from the protein and the protons from solvent water. In general, the evolution of longitudinal magnetizations of a system can be described by

$$\frac{dM_z}{dt} = -R * (M_z - M_{eq}) + k * M_z, \tag{1}$$

where M_z is a vector which represents the magnetizations of n protein protons and one type of solvent protons; M_{eq} is the magnetization vector of the protons in the equilibrium state; R is the longitudinal relaxation matrix and k is a matrix representing the exchange rates between labile protons and water protons. The diagonal and off-diagonal elements of R are expressed as

$$R_{i,i} = \sum_{j \neq i} \frac{\gamma^4 \hbar^2}{r_{ij}^6} [J(0) + 3J(\omega) + 6J(2\omega)], \tag{2}$$

$$R_{i,j} = \frac{\gamma^4 \hbar^2}{r_{ij}^6} [-J(0) + 6J(2\omega)], \tag{3}$$

where $r_{i,j}$ is the distance between protons i and j, γ is the gyromagnetic ratio, $\hbar = h/2\pi$ and h is the Planck's constant, and $J(\omega)$ is the spectral density function. The spectral density function is assumed to have the following simplest form (Lipari and Szabo 1982):

$$J(\omega) = S^2 \frac{\tau_m}{1 + (\omega\tau_m)^2} + (1 - S^2) \frac{\tau_e}{1 + (\omega\tau_e)^2}, \tag{4}$$

where S^2 is the generalized order parameter, τ_m is the overall tumbling time of the protein molecule and τ_e the effective correlation time. When considering the dipolar interaction between two protons in a methyl group, the order parameter is scaled down by a factor of 4 due to the rapid rotation of the methyl group along its C_3 symmetry axis.

The elements of the k matrix are given by

$$k_{i,i} = -k_{ex}(i,w), \quad k_{i,n+1} = k_{ex}(i,w)/f_w, \tag{5a}$$

$$k_{n+1,i} = k_{ex}(i,w), \quad k_{n+1,n+1} = -\sum_{i=1}^{m} k_{ex}(i,w)/f_w, \tag{5b}$$

where $k_{ex}(i,w)$ is the apparent exchange rate from the ith labile proton to water, f_w is the molar fraction of water, and m is the total number of labile protons in a protein molecule.

When water proton magnetization (M_{wz}) is inverted to the $-z$ direction, it rapidly returns back to the equilibrium state. During the rapid recovering period, the magnetization evolution cannot be described by Eq. 1. Instead, it is expressed as (Chen et al. 2000)

$$M_{wz}(t) = M_{weq}\tanh[R_D(t - t_0)], \quad (6)$$

where R_D is a constant reflecting the radiation damping strength, t_0 is a latency interval which is the time required for radiation damping to rotate the nearly inverted magnetization to the transverse plane, and M_{weq} is the equilibrium magnetization of water protons.

Within a small interval τ_j from time t_j to t_{j+1} during the recovering period, the water proton magnetization can be described approximately by a single exponential equation:

$$M_{wz}(\tau_j) = [M_{wz}(t_j) - M_{weq})]\exp(-R_j\tau_j) + M_{weq}, \quad (7)$$

where R_j is the apparent relaxation rate of water protons in the jth interval. The profile described by Eq. 6 agrees very well with the one approximated by Eq. 7 with an interval size of 1 ms (Fig. S1). Therefore, the evolution of proton magnetizations for protein plus water spins can be analyzed using Eq. 1 in each small time interval during the recovery period of water magnetization. After the recovery period, the magnetization evolution is described exactly by Eq. 1 during the rest of the mixing time.

Results and discussion

Water relaxation, radiation damping and steady-state water magnetization

The longitudinal relaxation rate of water (R_{1w}) in the ubiquitin sample was measured to be 0.3 s^{-1}. The R_{1w} values for two ACP samples were also found to be about 0.3 s^{-1} too, indicating R_{1w} is insensitive to salt concentration and pH. The radiation damping parameters R_D and t_0 for the ubiquitin sample were 309 s^{-1} and 9.3 ms, respectively, when measured with an inter-scan delay of 30 s. The radiation damping profile obtained with an inter-scan delay of 2 s could be roughly fitted to Eq. 6, yielding $R_D = 245$ s^{-1} and $t_0 = 13.9$ ms, which shows that the radiation damping effect is dependent on the inter-scan delay. For the ACP sample at pH 6.92, $R_D = 384$ s^{-1} and $t_0 = 12.0$ ms, and for the ACP sample at pH 7.47, $R_D = 368$ s^{-1} and $t_0 = 13.4$ ms when measured with an inter-scan delay of 2 s. The fractional steady-state water magnetizations at an inter-scan delay of 2 s were 0.78 and 0.84 for the ubiquitin and ACP samples, respectively.

HX during the mixing period

Under the conditions of $R_D = 309$ s^{-1} and $t_0 = 9.3$ ms, we generated the apparent water relaxation rate (R_j) for each time interval of 1 ms in the first 20 ms based on Eqs. 6, 7. Using R_j, relaxation matrix R and exchange matrix k, the magnetization evolution in the presence of radiation damping during the mixing period was simulated numerically for ubiquitin. In the absence of radiation damping, the magnetization evolution was simulated using Eq. 1. Except for the protons in –COOH groups, all other ubiquitin protons (in total 628) were included in our simulations. The difference of the magnetization for a labile proton in the presence (M_R) and absence (M_O) of radiation damping ($M_R - M_O$), represents the magnetization transferred from water to the labile proton. We defined the exchange peak intensity, I_{EX}, as $(M_R - M_O)/2$. In the first simulation, we assumed the HX rate only for A46 was 10 s^{-1} and the rates for all other backbone amides were zero. The I_{EX} for the H_N of A46 is nearly zero in the first 8 ms, then linearly increases with τ_{mix} in the second period, and slowly increases to reach a maximum number in the third period (Fig. 1a, filled circle). After that, I_{EX} decreases with the further increase of τ_{mix}. This dependence of I_{EX} on τ_{mix} represents the typical HX peak intensity profile that is measured with the scheme shown in Fig. 6.

From the simulation under the conditions of $R_D = \infty$ and $t_0 = 0$ ms (i.e., water magnetization is in the equilibrium state at time zero), we found that the dependence of I_{EX} on τ_{mix} (Fig. 1a, dashed line) is very similar to the one obtained under the conditions of $R_D = 309$ s^{-1} and $t_0 = 9.3$ ms but without the initial lag period (Fig. 1a, filled circle). This HX peak intensity profile represents the typical profile that is measured using the WEX pulse schemes (Mori et al. 1994, 1996b; Fitzkee et al. 2011). After a horizontal shift of 9.3 ms, the two profiles overlay very well during the time from ~15 to 300 ms (Fig. 1a). Actually, the horizontal shift is determined by t_0 (or radiation damping) and is independent of HX rates, which was confirmed by simulations.

The profile obtained under the conditions of $R_D = \infty$ and $t_0 = 0$ ms was fitted very well to the equation previously derived from an isolated two-spin system (Jeener et al. 1979; Mori et al. 1994) (Fig. 1b),

$$\frac{I_{EX}(t)}{I_{ref}} = \frac{f * k_{ex}}{R_1 + k_{ex} - R_{1w}}[\exp(-R_{1w}t) - \exp(-(R_1 + k_{ex})t)], \quad (8)$$

where k_{ex} is the HX rate, R_1 is the relaxation rate of an amide proton, I_{ref} is the equilibrium magnetization of the amide proton, and f is the fractional steady-state water magnetization (i.e., the ratio of the steady-state to the

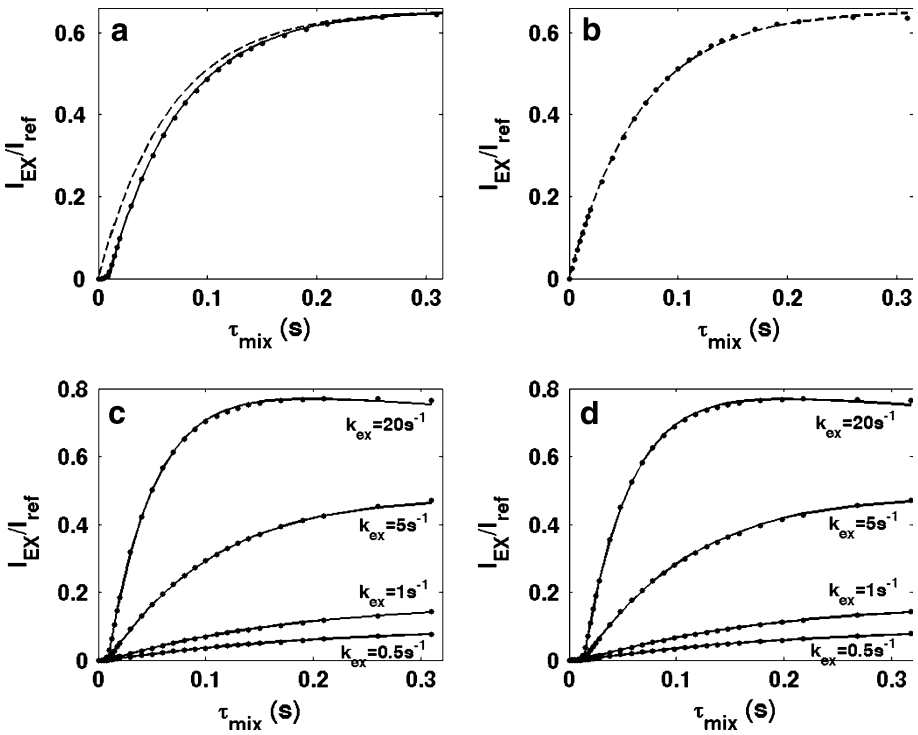

Fig. 1 Dependence of I_{EX}/I_{ref} on τ_{mix} under different conditions. **a** Peak intensity profiles obtained under the conditions of $R_D = 309$ s^{-1} and $t_0 = 9.3$ ms (*filled circle*) and $R_D = \infty$ s^{-1} and $t_0 = 0$ ms (*dashed line*), and the *solid line* represents the result of horizontally shifting the *dashed line* by 9.3 ms. **b** Comparison of the peak intensity profile simulated under the condition of $R_D = \infty$ s^{-1} and $t_0 = 0$ ms (*dashed line*) and the best fit to Eq. 8 (*filled circle*). **c** Peak intensity profiles simulated with different input k_{ex} values under the conditions of $R_D = 309$ s^{-1} and $t_0 = 9.3$ ms (*filled circle*) and their best fits to Eq. 9 (*solid lines*). **d** Peak intensity profiles simulated with different input k_{ex} values under the conditions of $R_D = 245$ s^{-1}and $t_0 = 13.9$ ms (*filled circle*) and their best fits to Eq. 9 (*solid lines*). In all simulations and curve fitting, R_{1w} was set to 0.3 s^{-1}

equilibrium water magnetizations). In analog to Eq. 8, the peak intensity profile measured using the pulse scheme shown in Fig. 6 should be described well by the following equation,

$$\frac{I_{EX}(t)}{I_{ref}} = \frac{f * k_{ex}}{R_1 + k_{ex} - R_{1w}}[\exp(-R_{1w}(t - t_0)) - \exp(-(R_1 + k_{ex})(t - t_0))], \quad (9)$$

where t_0 is the latency interval.

Figure 1c shows the simulated peak intensity profiles for A46 assuming 4 different k_{ex} values: 20, 5, 1 and 0.5 s^{-1} under the conditions of $R_D = 309$ s^{-1} and $t_0 = 9.3$ ms, while Fig. 1d shows the profiles under the conditions of $R_D = 245$ s^{-1} and $t_0 = 13.9$ ms, which represents the case where the inter-scan is 2 s. The intensity profiles were fitted very well to Eq. 9 for the data points with delays larger than t_0 under both radiation damping conditions. In the fitting here and thereafter, R_{1w} was fixed at 0.3 s^{-1}. The extracted k_{ex} values were 3–4% smaller than the input values. However, the extracted R_1 values were about 20–25% smaller than the input auto-relaxation rate of the amide proton of A46. Note that the input R_1 value of the jth proton corresponds to the jth diagonal element in the R matrix, which is dominated by $J(0)$. For an isolated system (i.e., a molecule with a single proton), the extracted R_1 and k_{ex} values were nearly identical to the input values. Therefore, the discrepancy between the extracted and input parameters is caused by the cross-relaxation among the amide proton of A46 and its proximal protons. The results show that HX rates can be measured in good accuracy using the pulse scheme shown in Fig. 6, but the auto-relaxation rates extracted from the curve fitting are very inaccurate.

Effects of exchange-relayed NOE and direct NOE on the measured HX rates

Besides direct HX, exchange-relayed NOE between an amide proton and a labile proton and direct NOEs between an amide proton and its proximal H_α protons that have nearly the same resonance frequencies as water can contribute to the measured k_{ex}. To evaluate the exchange-relayed NOE effect, we performed simulations assuming that the HX rate for G47 was zero but the HX rate of A46 varied from 5 to 5,000 s^{-1}. Note that the amide protons of A46 and G47 are separated by 3.1 Å, their simulated cross-relaxation rate was 0.42 s^{-1} and the simulated

(or input) R_1 value of G47 was 4.3 s^{-1}. For comparison, we did another simulation for the pure exchange effect by setting the HX rate for G47 to 0.42 s^{-1} and the HX rates for other amides to zero. The resultant peak intensity profiles for G47 are shown in Fig. 2. The peak intensity profiles originating from the pure exchange have a curve-down shape (square). On the other hand, the profiles of the exchange-relayed NOE peak have a curve-up shape and cannot fit well to Eq. 9 when the exchange rate for A46 is below 50 s^{-1} (Fig. 2, open circle). When the HX rate for A46 is 200 s^{-1}, the peak intensity profile resembles a straight line, which was realized previously by Fitzkee et al. (2011), and could not fit well to Eq. 9 (Fig. 2, filled circle). When k_{ex} = 1,000 s^{-1}, the intensity profiles could fit very well to Eq. 9 with a fixed R_{1w} value of 0.3 s^{-1}, and the extracted k_{ex} value for G47 was 0.42 s^{-1}, same as expected from the cross-relaxation rate. However, the extracted R_1 value was 1.65 s^{-1}, about 62% smaller than the input R_1 value (4.3 s^{-1}). The result for k_{ex} = 5,000 s^{-1} was the same as that for k_{ex} = 1,000 s^{-1}. From the intensity profile of the pure exchange peak, we found that the extracted k_{ex} and R_1 values were 0.42 and 3.5 s^{-1}, respectively. The R_1 value obtained from the pure HX profile is about 20% smaller than the input value. When both the pure exchange and exchange-relayed NOE effects exist, the extracted R_1 value is larger than 1.65 but smaller than 3.5 s^{-1}. Even when HX rates (e.g., 5,000 s^{-1}) are much larger than R_D (i.e., hydroxyl or labile protons and water protons are inverted at the same time), the extracted R_1 value is still 62% smaller than the input value although the intensity profile looks like that resulting from the pure HX effect. Therefore, it is possible to differentiate exchange-relayed peaks from pure exchange peaks by checking the shape of the intensity profiles and extracted R_1 values. For a folded protein, the R_1 value of an amide proton should not be significantly smaller than τ_m s^{-1}, where τ_m is the overall tumbling time of the protein in the unit of ns, especially for the residues in the regular secondary structural elements. For example, τ_m = 4 ns for ubiquitin, and the simulated R_1 values of amide protons are in the range of 2.7–6.9 s^{-1}. When the extracted R_1 value is around zero or much smaller than expected, the extracted k_{ex} may be contaminated by the exchange-relayed NOE contribution.

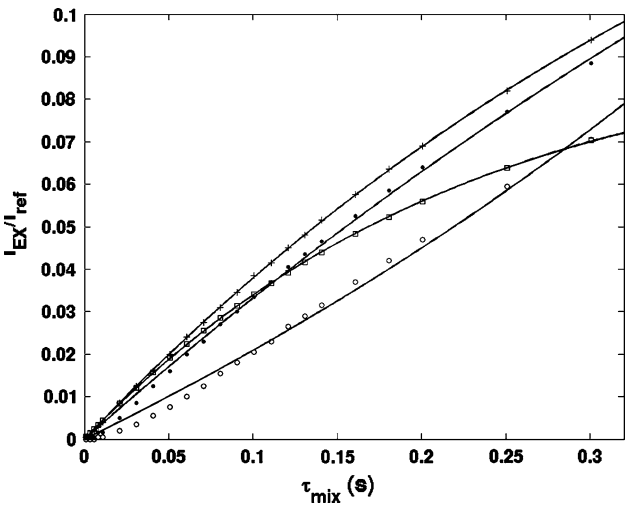

Fig. 2 Dependence of I_{EX} of G47 on τ_{mix}. The exchange-relayed peak intensities were obtained by assuming k_{ex} = 0 for G47 and k_{ex} = 1,000 (*plus symbol*), 200 (*filled circle*), and 20 s^{-1} (*open circle*) for A46. The direct exchange peak intensities were obtained by assuming k_{ex} = 0.42 s^{-1} for G47 and k_{ex} = 0 s^{-1} for other backbone amides (*square*)

A protein proton resonating at a frequency close to the water frequency can be inverted by the radiation damping field (Miao et al. 1999). Thus this partially or completely inverted proton may give rise to the direct NOE effect. The degree of the inversion depends on the frequency difference between a protein proton and water protons ($\Delta\nu$), and the inversion profile is determined by R_D (Fig. 3a). When $|\Delta\nu| = 0.67R_D/\pi$, 95% magnetization is not perturbed or 5% is inverted. The frequency difference at a 5% inversion level is defined as $\Delta\nu_{5\%}$. For a H_α proton with a $|\Delta\nu|$ value smaller than $\Delta\nu_{5\%}$, its direct NOE contribution to the measured HX rates should be considered. Besides $\Delta\nu$, the spatial location and dynamics of a H_α proton also strongly influence the direct NOE contribution. Thus, it is difficult to predict which amides suffer from the direct NOE effect in the measurements of HX. Fortunately, the peak intensity profile resulting from the pure HX effect is quite different from that resulting from the direct NOE effect (Fig. 3b), allowing us to distinguish between these two effects. When simulating the intensity profiles from the direct NOE effect, we assumed that $\Delta\nu = 0$ for the H_α of D21 and the HX rates were zero for D21 and T22. In the simulation, the input auto-relaxation R_1 rates were 4.1 and 6.0 s^{-1} for amide protons of D21 and T22, respectively, while the input cross-relaxation rates for D21H_α–D21H_N and D21H_α–T22H_N were 0.30 and 1.25 s^{-1}. The input relaxation rates were calculated from Eqs. 2 and 3 using the assumed dynamic parameters. Fitting the simulated intensity profiles to Eq. 9 with a fixed R_{1w} value of 0.3 s^{-1}, we obtained apparent k_{ex} values of 0.39 and 1.41 s^{-1} and R_1 values of 6.3 and 13.1 s^{-1} for D21 and T22, respectively. The extracted k_{ex} values are close to the respective input cross-relaxation rates. However, the extracted R_1 values are >50% larger than the respective input values. In comparison, we also simulated the intensity profiles resulting from the pure HX effect for D21 and T22 (Fig. 3b) by assuming the HX rates were 0.30 and 1.25 s^{-1}, respectively and all H_α spins are far away from water. For the pure exchange profiles, the extracted k_{ex} values were 0.38 and 1.21 s^{-1}, and the R_1 values were 2.8 and 4.9 s^{-1} for D21 and T22,

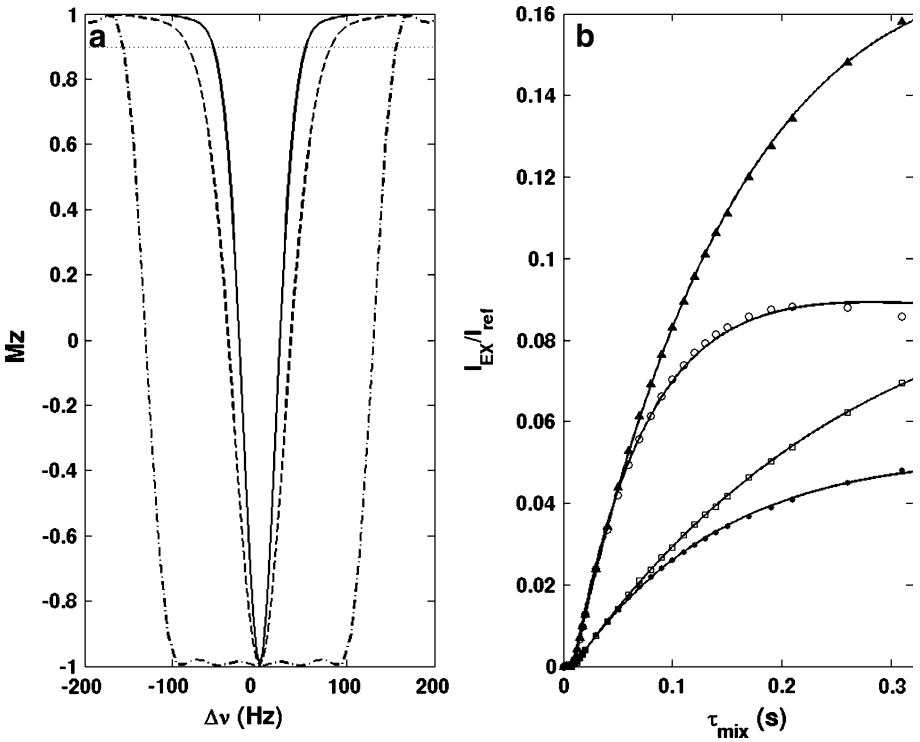

Fig. 3 **a** Inversion profiles of a 20 ms IBURP2 selective pulse with a maximal *rf* of 248 Hz (*dash-dot line*) and radiation damping fields for $R_D = 385$ Hz (*dashed line*) and $R_D = 250$ Hz (*solid line*). The *dotted line* at $M_z = 0.9$ indicates the 5% inversion level (note that 1 and -1 mean 0 and 100% inversion, respectively). **b** Simulated exchange peak intensity profiles resulting from pure HX effects for D21 (*square*) and T22 (*triangle*), and from direct NOE effects for D21 (*filled circle*) and T22 (*open circle*). In the case of the pure HX effect, the HX rates for D21 and T22 were assumed to be 0.3 and 1.25 s^{-1} and no H_α protons are close to water. In the case of the direct NOE effect, the H_α of D21 was assumed to be fully inverted by the radiation damping field. The cross-relaxation rates for $D21H_\alpha$–$D21H_N$ and $D21H_\alpha$–$T22H_N$ were 0.30 and 1.25 s^{-1}, respectively

respectively, which are 20–30% smaller than the input R_1 values.

In the case where there is only the direct NOE effect between an amide and its proximal H_α, the intensity profile can still be described by Eq. 9 but the R_{1w} should be substituted with a quite different relaxation rate of H_α (Mori et al. 1994). This explains why the R_1 values extracted with the use of a fixed R_{1w} value of 0.3 s^{-1} are much larger than the input ones. On the basis of H_α chemical shifts and extracted R_1 values, we should be able to know if the extracted k_{ex} values are free of the direct NOE contribution. In both the direct NOE and exchange-relayed NOE cases, the observed exchange signals are caused by the NOE instead of the HX effect. In the direct NOE case, the inverted H_α magnetization quickly goes back from the $+z$ to the $-z$ axis during the mixing period since other protein protons are aligned along the $-z$ direction. In the exchange-relayed NOE case, the inverted labile proton (e.g., hydroxyl proton) magnetization remains along the $+z$ axis since it rapidly exchange with water protons that are in the equilibrium (or steady) state. Therefore, the peak intensity profiles and extracted apparent R_1 values for these two cases are quite different. Because of the differences, one can identify which residues may be contaminated by the direct NOE or the exchange-relayed NOE contributions.

For our ubiquitin sample, the half-height line width was estimated to be $\sim$80 Hz from the measured R_D value (309 s^{-1}) (Mao and Ye 1997), and the water magnetization could be completely inverted within 20 ms by radiation damping on an 800 MHz spectrometer equipped with a cryoprobe. For the same water signal, about 97% water magnetization can be inverted using a 20 ms IBURP2 shaped pulse (Geen and Freeman 1991), which is one of the best inversion pulses in terms of selectivity. Comparing the excitation profiles of the selective pulse and radiation damping field (Fig. 3a), we see that much fewer H_α protons can be inverted by the radiation damping field than by the selective pulse. Therefore, radiation damping has much higher selectivity than any existing selective pulses when the same degree of water magnetization inversion is achieved.

To accurately measure small HX rates, it is necessary to use a long mixing time (τ_{mix}). Due to proton–proton cross-relaxation, however, the data points beyond a certain mixing time cannot fit to Eq. 9 (Fig. S2) and become

useless. Because HX intensity profiles depend on k_{ex}, R_1 and τ_{mix}, it is impossible to find an ideal τ_{mix} suitable for all the residues in a protein. According to simulations, a mixing time of $\sim$500 ms should be long enough for fully protonated samples. For a given HX rate and τ_{mix}, the HX peak intensity decreases with the increase of protein size (Fig. S2). Also, the experimental sensitivity decreases with protein size. Therefore, the EXSY-based methods are suitable for relatively small proteins for the measurement of relatively small HX rates ($\sim$0.1–1 s^{-1}). For medium-sized proteins (20–30 kDa), it is likely difficult to obtain accurate HX rates below 0.5 s^{-1} when non-deuterated protein samples are used. In order to further extend τ_{mix}, one has to reduce ^{1}H–^{1}H cross-relaxation rates by partial or complete deuteration. Recently, it has been showed that the peak intensity profiles still fit well to Eq. 8 when the mixing time is as high as 500 ms for a 36 kDa perdeuterated protein (Fitzkee et al. 2011).

Ubiquitin

We first tested the experiment using ubiquitin of which the high resolution structure is known. Consistent with simulations, the peak intensity profiles were fitted very well to Eq. 9 except for the amides with significant contributions from the exchange-relayed NOEs (Fig. 4a, b). The extracted HX rates and R_1 values are given in the supplementary table (Table S1). The HX rates measured with the use of an inter-scan delay of 2 s were the same (within experimental errors) as those measured with the use of a much longer delay (12 s), indicating that the measurements are independent of the inter-scan delay. This is because the observed signals are from the transfer of water magnetization to amide protons. On the other hand, the HX signal intensities are dependent on the steady-state water magnetization or inter-scan delay. So the inter-scan delay cannot be too short and a delay of 2 s seems to be a good choice.

For most residues with k_{ex} values $> \sim 1$ s^{-1}, the HX rates measured by our method agree well with those by the CLEANEX method (Table S1). The k_{ex} values of V17 and T22 were $\sim$1.6 and $\sim$1.0 s^{-1} as measured using the method proposed here, but V17 and T22 were not detectable in the CLEANEX spectra because their HX rates are too small ($< \sim 1$ s^{-1}). Thus the measured k_{ex} rates for these two residues should be dominated by the direct NOE contribution. Many residues had k_{ex} values smaller than 1 s^{-1}, but they could not be measured by the CLEANEX method. For these residues, we have to use an alternative method to determine if the measured apparent exchange rates are from the pure HX, direct NOE or exchange-relayed NOE effect. According to the simulation results, we can identify the residues with significant direct NOE or exchange-relayed NOE contributions from the H_α chemical shifts and extracted R_1 values. Relative to water, the H_α resonant frequencies of T7, T14, E16, V17, D21, T22, I44 and K48 are <52 Hz ($\Delta\nu_{5\%}$). For these residues and their adjacent residues, the measured HX rates might contain the direct NOE contributions. Furthermore, the apparent R_1

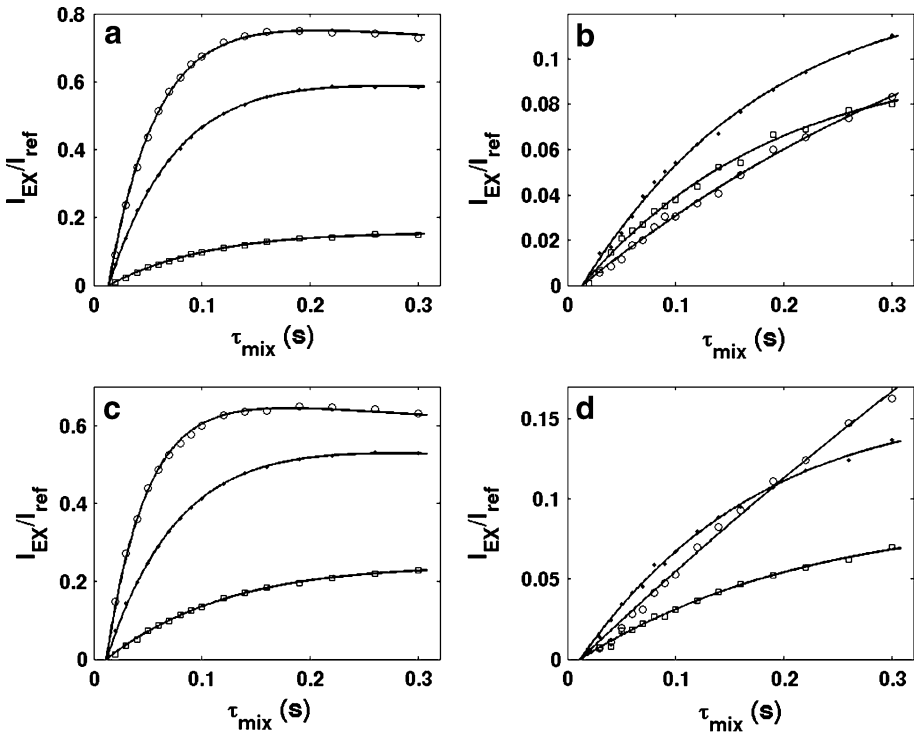

Fig. 4 Experimental peak intensity profiles and their best fitting curves for ubiquitin (**a** *open circle* for T66, *filled circle* for A46 and *square* for V17; **b** *filled circle* for E51, *square* for Q49 and *open circle* for T66) and for *me*ACP (**c** *open circle* for N72, *filled circle* for A66 and *square* for H21; **d** *filled circle* for M46, *open circle* for D37 and *square* for E17). For T66 of ubiquitin and D37 of *me*ACP, the intensity profiles deviate from the ones with the pure exchange effect

values for only E16, V17, E18, T22, I23 and F45 are significantly larger than the average (Table S1). Thus the measured k_{ex} values for these six residues are very likely to be dominated by the direct NOE effect. Using the CLEANEX experiment, only V17 and T22 could be confirmed to have the direct NOE contribution.

Residues L8-T12, A46, L73-G75 had k_{ex} values larger than 1 s^{-1}. L8-G10 and A46 are located in loop regions, while residues L73-G76 are in the unstructured C-terminal end. Except for G76, the measured HX rates for these residues agree well with the structure. The fact that the HX rate for G76 is much smaller than that for G75 is caused by the effect of the negatively charged C-terminus (COO^-) (Bai et al. 1993). Several backbone amides are predicted to be involved in hydrogen bonding (G10, E51, R54 and T55), but they displayed significant amide hydrogen exchange and had normal apparent R_1 values. These residues are located in the reverse turns and their hydrogen bonding may be much weaker than other residues in the regular secondary structure elements. Three residues (Q2, T7 and S57) had k_{ex} values smaller than 0.3 s^{-1} and apparent R_1 values smaller than 1 s^{-1}. Very likely, the k_{ex} values for these residues are dominated by the contribution from exchange-relayed NOEs instead of pure HX. According to the x-ray structure (PDB: 1UBQ), indeed, each of these amide protons has at least one very labile proton nearby (<3.5 Å). Consistently, they are predicted to use their amides to form hydrogen bonds (Vijay-Kumar et al. 1987) and should not have detectable HX rates. The amide proton of Q62 is predicted to be very close to the hydroxyl proton of S65 (1.95 Å corresponding to a cross-relaxation rate of 1.9 s^{-1}). However, the measured k_{ex} (0.43 s^{-1}) was much smaller than 1.9 s^{-1} and did not show significant exchange-relayed NOE contribution. This may be caused by the slight difference of side-chain orientations in the crystal and solution states or/and by a significant difference in the assumed ($S^2 = 0.5$) and actual order parameters. Thus, accurate prediction of exchanged-relayed NOE contribution is impossible from the structure.

Application to ACP

Acyl carrier protein (ACP) is involved in the biosynthesis of fatty acid, nonribosomal peptide and polyketide as the carrier of biosynthetic intermediates. Most ACPs adopt a canonical four-helix bundle structure and are highly dynamic (Chan and Vogel 2010). The dynamic feature is assumed to play important roles in substrate delivery and interactions of ACP and ACP synthase. Recently, we have determined the structure of the ACP domain of iterative polyketide synthase CalE8 (*me*ACP) that initiates biosynthesis of the enediyne natural product calicheamicins in *Micromonospora echinospora* (Lim et al. 2011). Different from other ACPs, this *me*ACP domain adopts a twisted three-helix bundle structure. As evidenced by heteronuclear NOEs, all three helices and the long loop between helices 1 and 2 are rigid, while loop-2 between helices 2 and 3 exhibits more flexibility on ns-ps timescale. The flexibility in loop-2 alone is insufficient for the protein to interact with its partner proteins since significant conformational changes are observed upon the interaction of ACP from *Bacillus subtilis* with ACP synthase (Parris et al. 2000). Here we apply the HX experiment shown in Fig. 6 to probe the dynamics on the second timescale.

The HX rates were measured at pH 6.92 and pH 7.47, respectively. Although overall tumbling time of *me*ACP (~7.5 ns which was estimated from ^{15}N relaxation times T_2 and T_1) is significantly larger than that for ubiquitin (~4 ns), the peak intensity profiles obtained at both pH values could be fitted very well to Eq. 9 except for the amides with significant contributions from the exchange-relayed NOE (Fig. 4c, d). The extracted k_{ex} and R_1 values are summarized in supplementary Table S2. Relative to water, the H_α resonant frequencies of only M69, N72 and A76 were <82 Hz ($R_D = 384$ Hz and $\Delta\nu_{5\%} = 82$ Hz). After taking into account the extracted R_1 values which are significantly larger than the average, we found that only N72 and T77 might have the direct NOE contribution to their measured k_{ex} values. Residues L16, L18, V23, V33, D37, R39, L44, Q53, R79 and A87 had apparent R_1 values smaller than 1 s^{-1} at pH 6.92. The measured HX rates for these residues might contain contributions from the exchange-relayed NOEs. However, it is impossible to know the pure HX rates from an experiment at a single pH. Conducting one more experiment at a higher pH, in principle, we can determine both direct HX and indirect HX contributions by assuming the direct HX rate is entirely base-catalyzed, i.e., proportional to 10^{pH} (Bai et al. 1993), while the indirect HX rates such as direct NOEs and exchange-relayed NOEs are independent of pH. For many residues, the ratios of k_{ex} values measured at the two pH values were about 3.5, agreeing with the predicted number from the pH difference ($10^{\Delta pH} = 3.55$) by assuming that there are no exchange-relayed and direct NOE contributions. If the exchange-relayed or/and direct NOE contributions exist, the ratio must be smaller than 3.55. Several residues (V19, F40, L41, V55, T77 and E80) showed k_{ex} ratios significantly smaller than 3.5, indicating the presence of exchange-relayed NOE or direct NOE contributions. Surprisingly, a large number of residues (L16, L18, R20, V23, E25, R26, A27, E28, G52, Q53, N56, A58, M62, G63, M81 and A87) had the ratios significantly larger than 3.5, which cannot be explained by the presence of the direct or/and exchange-relayed NOE effects. Interestingly, all of these residues are located in α-helices. This result can be interpreted only by the assumption that the populations of the unfolded species (or open states) are slightly

different at the two pH values although the HSQC spectra are very similar. Consequently, we did not calculate the exchange-relayed NOE contributions even for those residues with k_{ex} ratios smaller than 3.5. At pH 6.92, many residues in the α-helices had conformational exchange contributions to the ^{15}N transverse relaxation (R_{ex}, data not shown), showing the presence of invisible states. The invisible state may correspond to unstructured conformations since the protection factors of many residues in the helices are smaller than 30 as shown below.

Unlike ubiquitin in which most amides located in regular α-helices and β-sheets had k_{ex} rates significantly smaller than 0.1 s^{-1}, only ~7% amides in *me*ACP displayed HX rates smaller than 0.1 s^{-1} at pH 6.92, while all amides showed HX rates larger than 0.3 s^{-1} at pH 7.47, indicating the helical structure is unstable in solution. From the measured k_{ex} values, we estimated the protection factors (Table S2; Fig. 5). The N-terminal region (A4-G14), middle part of loop-2 (S65-T75) and C-terminal region (E91-E96) are less protected than the three helices and loop-1. Except for D36, loop-1 is similar to the helices in protection factors. The result shows that loop-1 has similar mobility to the regular helices, which is consistent with the flexibility detected on ns-ps timescales from our previous study (Lim et al. 2011). The protection factors of all amides in the regular secondary structural elements are smaller than 85, much smaller than the values observed in other proteins (Mori et al. 1997; Fitzkee et al. 2011). They are also much smaller than the values for the ACP of *E.coli* which are larger than 1,000 for most amides (Andrec et al. 1995). The low protection factors show that *me*ACP is highly dynamic on the second timescale. This high mobility over the entire protein allows it to interact with substrate and enzymes via easy conformational changes. The low protection factors for all residues in the three helices imply that there are unfolded species, which are invisible but can be detected by the relaxation dispersion technique (we are now performing the relaxation dispersion study). The conformational changes are probably achieved through the unfolded intermediates.

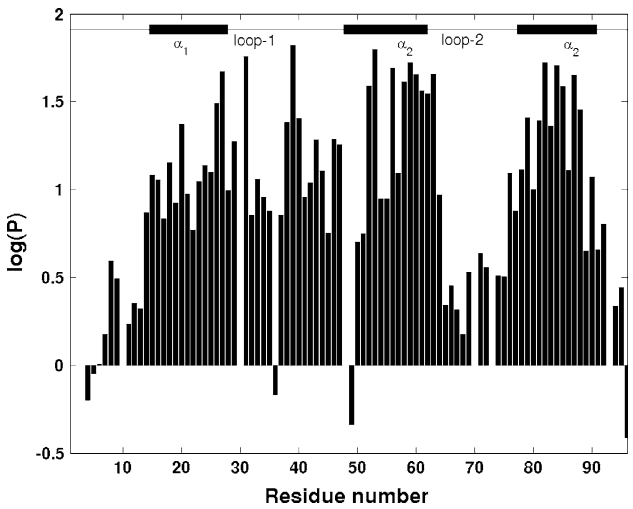

Fig. 5 Protection factors of amides in *me*ACP. When the protection factors of an amide were available at two pHs, their average value was used

Conclusion

Radiation damping is troublesome in many cases, but it can be used to selectively invert water protons. Although magnetization evolution of a protein system is a complicated process during the rapid water recovery period in the presence of radiation damping, the magnetization transfer from water to amide protons through the amide hydrogen exchange are approximately described by four parameters: exchange rate (k_{ex}), apparent relaxation rate for an amide proton (R_1), latency interval (t_0) and relaxation rate of water proton (R_{1w}). The dependence of the exchange peak intensity on these four parameters is approximately expressed by Eq. 9 when the mixing time is below a certain limit. This limit is beyond the initial mixing period. With the use of a long mixing time, HX rates as small as 0.1 s^{-1} can be measured for small and medium-sized non-deuterated proteins using the pulse scheme developed here. Although the direct NOEs and exchange-relayed NOEs contribute to the measured exchange rates, the residues having such significant contributions often can be identified from the shapes of the peak intensity profiles or/and from the extracted apparent R_1 values together with H_α chemical shifts, namely the residues with the R_1 values around zero should have significant exchange-relayed contributions to the measured exchange rates, while the residues with R_1 values much larger than the average should have the direct NOE contributions. The method proposed here has been demonstrated on ubiquitin and applied to a highly dynamic ACP. The experimental data further support the conclusions drawn from numerical simulations.

Our *me*ACP k_{ex} data measured at pH 6.92 and 7.47 demonstrate that HX rates close to 0.1 s^{-1} can be measured accurately. In addition, quantification of indirect HX contributions is difficult because the population of the open state of *me*ACP may change with pH even in a small pH range. All amide protons in *me*ACP have protection factors smaller than 85, indicating *me*ACP is highly flexible on the second timescale although only loop-2 is dynamic on the ns-ps timescale. This result shows no necessary correlation between dynamics on different timescales. The high flexibility should have important implications to the function of *me*ACP.

Materials and methods

Samples

^{15}N-labeled *me*ACP domain was expressed in *E.coli* and purified by affinity columns as described previously (Lim et al. 2011). The purified protein was concentrated to a concentration of $\sim$1 mM in a buffer of 50 mM NaCl, 20 mM phosphate, 1 mM DTT at a desired pH. Two ACP samples, one at pH 6.92 and the other at pH 7.47, were used in this study. A standard sample of ^{13}C,^{15}N-labeled ubquitin in a buffer of 20 mM phosphate and 130 mM NaCl at pH 6.8 was used too.

Pulse scheme

In this work, we used the radiation damping effect to select water magnetization. The pulse scheme used here is a modified version of the previous work by Bockmann et al. (1996) (Fig. 6). Two interleaved data sets were acquired, one in the presence of gradients G_2 and G_0, the other in the absence of G_2 and G_0 during the mixing period. Water proton magnetization returns back to the equilibrium state in tens of ms in the absence of G_2 and G_0, while it takes several seconds to reach full recovery in the presence of G_2 and G_0 (Bockmann et al. 1996; Fitzkee et al. 2011). Once water protons are recovered but protein protons are still in the inverted state, magnetization transfer from water to labile protein protons can take place effectively via HX. On the other hand, the magnetization transfer is minimized when both water and protein protons are in the inverted state. Because the relaxation of most protein spins is not affected by G_2 and G_0, taking the difference of the two interleaved data sets can remove the signals originating from the protein spins and obtain the signals resulting from HX. After the first INEPT, water magnetization is normally flipped back by a selective pulse. When the selective pulse was used, we found artifacts in the difference spectrum even with the insertion of a strong gradient pulse just after the selective pulse (at least on our spectrometer). The artifacts could be suppressed by phase cycle of the first ^{1}H 90° hard pulse and the selective pulse together. Note that the phases of the selective pulse should be different in the presence and absence of G_2 and G_0 since water protons are aligned differently after the mixing period. In addition, the loss of water magnetization can be different in the two interleaved experiments if the selective pulse is not calibrated properly in terms of small angle shift and pulse width. Here we used a short delay (10 ms) during which the water magnetization can return back to its steady state from the transverse plane. On high field spectrometers ($\geq$800 MHz) equipped with cryoprobes, the recovery times were less than 10 ms for all the samples we tested. If the recovery time is significantly longer than 10 ms, use of a selective pulse is recommended.

NMR spectroscopy

All NMR experiments were carried out on a Bruker 800 MHz NMR spectrometer equipped with a cryoprobe at 25°C. When HX rates were measured using the pulse scheme shown in Fig. 6, we recorded two sets of data for ubiquitin, one with an inter-scan delay of 2 s and the other with a delay of 12 s. For each *me*ACP sample, only one set of data was collected with an inter-scan delay of 2 s. For the data set with a shorter inter-scan delay, we utilized the following 15 mixing times: 20, 30, 40, 50, 60, 70, 80, 90, 100, 120, 140, 160,190, 220, 260 and 300 ms. For the data set with a longer inter-scan delay, we used four mixing times: 20, 50, 100 and 160 ms. For each mixing time, two interleaved data sets were collected, one with radiation damping and one with the suppression of the radiation

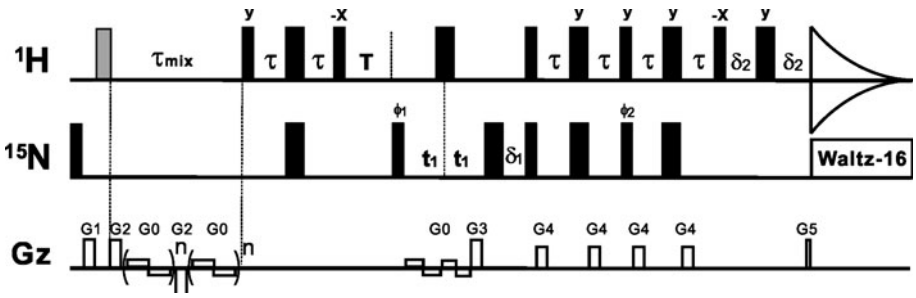

Fig. 6 Pulse scheme for the measurement of HX rates. All narrow (wide) rectangular pulses are applied with a flip angle of 90° (180°). The first ^{1}H pulse (*gray*) has a flip angle close to 180° (in the range of 170°–180°). Adjustment of this pulse can change the latency interval t_0. The carriers are centered at 4.7 and 119 ppm for ^{1}H and ^{15}N, respectively. Delays used were: $\tau = 2.4$ ms, $T = 10$ ms, $\delta_1 = 0.5$ ms and $\delta_2 = 0.5$ ms. The phase cycling used was: $\phi_1 = x, -x$ and rec $= x, -x$. Quadrature detection in the F1 dimension used the enhanced sensitivity pulsed field gradient method (Kay et al. 1992). The duration, peak strength and shape of the gradients were: $g_1 =$ (1 ms, 2.5 G/cm, Sine), $g_2 =$ (1 ms, 25 G/cm, Sine), $g_3 =$ (0.5 ms, 40 G/cm, *Smoothed Square*), $g_4 =$ (2.18 ms, 8.5 G/cm, Sine), and $g_5 =$ (0.5 ms, 4.05 G/cm, *Smoothed Square*). During the mixing period, $g_0 =$ 1.5 G/cm in the first experiment, while $g_0 = 0$ G/cm in the second experiment

damping. Each data set comprised of 100 × 640 complex points in the ^{15}N and ^{1}H dimensions, corresponding to acquisition times of 48.8 and 57.3 ms, respectively. Each FID was acquired using 2 scans. The total experimental times for the delays of 2 and 12 s were about 7.5 and 11 h, respectively. For each sample, a reference spectrum was recorded with the scheme shown in Fig. 6 by removing the first ^{1}H pulse and the mixing period and using a long inter-scan delay of 12 s. When the HX rates for ubiquitin were measured with the CLEANEX method (Hwang et al. 1997, 1998), following mixing times were used: 5, 8, 12, 16, 20, 25 ms; except for inter-scan delay and scan number which were 2 s and 32 respectively, other acquisition parameters were the same as those used for the experiment developed here.

The radiation damping profile was measured using a two-pulse scheme, π–t–Gr–α–Acq, where π is a 180° ^{1}H pulse, t is a delay, Gr is a pulsed gradient of 1 ms at 25 G/cm, and α is a 1 μs pulse. The data were recorded using one scan, eight dummy scans and an acquisition time of 57 ms. First, the FID was acquired by setting $t = 1$ s; the time at which the FID reaches the maximum amplitude was identified and defined as t_{amp}. Second, FIDs were recorded for a series of delays from 1 to 60 ms. Finally, the amplitudes of FIDs at t_{amp} were used to draw the radiation damping profiles. For the ubiqitin sample, two radiation damping profiles were recorded using inter-scan delays of 2 and 30 s, respectively. For each *me*ACP sample, one radiation damping profile was acquired using an inter-scan delay of 2 s. The radiation parameters R_D and t_0 were obtained by fitting the profiles to Eq. 6.

The longitudinal relaxation rate of water (R_{1W}) was measured using the saturation recovery method described by Fitzkee et al. Water was saturated for 5 s using a train of high power 120° pulses separated by 5 ms. During the recovery period, a pulsed gradient of 1 ms at 40 G/cm was applied, followed by a weak gradient of 1 G/cm. Recovery times of 50, 100, 200, 400 and 800 ms were used to measure the recovery signal intensities. FID amplitudes at t_{amp} instead of peak volumes were used to determine R_{1W} by assuming the recovery follows a single exponential function.

To measure the degree of water recovery (or fractional steady-state water magnetization), the pulse scheme shown in Fig. 6 was modified by inserting one delay followed by a 1 μs ^{1}H pulse just before the acquisition. FIDs were acquired using one scan and 8 dummy scans. The FID amplitudes at t_{amp} for the delays of 2 and 30 s were used to calculate the degree of water recovery.

NMR data analysis

The interleaved 2D data sets were separated and the difference of the two separated data was processed using the NMRPipe package (Delaglio et al. 1995). The ^{15}N time-domains were doubled by linear prediction prior to the application of a cosine-squared window function. After zero-filling and Fourier transformation, the final data sets consisted of 1,280 and 512 points along the F2 and F1 dimensions, respectively. Peak picking was done in NMRDraw. Peak intensities were determined by adding the signal heights of 4 × 4 points around the peak center point. For each peak, the peak intensities were fitted to Eq. 9 using an in-house written matlab script. The 95% confidence interval on each fitting parameter was considered as the fitting error.

Protection factor

The protection factor was calculated from the ratio of the 'random coil' HX rate (k_{rc}) to the measured HX rate. k_{rc} was estimated from the following equation:

$$\log k_{rc} = \log k_B + \log B_L + \log B_R, \tag{10}$$

where $\log k_B = 9.95\ \text{M}^{-1}\text{Min}^{-1}$ (Connelly et al. 1993), $\log B_L$ and $\log B_R$ are the correction factors for side-chains which are taken from the published data (Bai et al. 1993). The effect of temperature on k_{rc} was corrected as described previously (Bai et al. 1993).

Numerical simulations

Except for the protons in –COOH groups, all other ubiquitin protons (in total 628) were included in our simulations. In the calculation of the relaxation matrix R, we made the following assumptions: $\tau_m = 4$ ns, $\tau_e = 50$ ps, $S^2 = 0.85$ for H–H vectors between any two backbone protons, $S^2 = 0.5$ for H–H vectors involved in any non-methyl side-chain protons and $S^2 = 0.5/4$ for methyl H–H vectors. Also, we assumed that the two CH_2 protons are chemically different, the three CH_3 protons are chemically equivalent and there is no cross relaxation between any protein protons and water protons. The distance between a pair of protons was calculated from the x-ray structure (PDB code: 1UBQ). Using the assumed dynamic parameters (τ_m, τ_e and S^2) and calculated H–H distances, we calculated spectral density functions, auto- and cross-relaxation rates from Eqs. 2–4, respectively.

For all backbone amide, side-chain $CONH_2$, and tryptophan side-chain NH groups, the HX rates were set to zero, unless indicated otherwise. For other labile protons, the HX rates were set to 1,000 s^{-1}. The elements of the k matrix in Eq. 1 were calculated from Eqs. 5a, 5b based on the assumed HX rates. The evolution of proton magnetizations was calculated by solving Eq. 1 numerically using an in-house written matlab script.

Acknowledgments This work was supported by a grant from the ministry of education, Singapore (R154000453112). The authors thank Lewis E. Kay for his seminal contributions to the NMR community. DY is immensely grateful to Lewis for his patient guidance in NMR experiment developments and data analyses when DY was working in his laboratory. DY is indebted to Lewis for his continuous support, encouragement and inspiration.

References

Andrec M, Hill RB, Prestegard JH (1995) Amide exchange rates in *Escherichia coli* acyl carrier protein: Correlation with protein structure and dynamics. Protein Sci 4:983–993

Bai YW, Milne JS, Mayne L, Englander SW (1993) Primary structure effects on peptide group hydrogen exchange. Proteins Struct Funct Genet 17:75–86

Bockmann A, Penin F, Guittet E (1996) Rapid estimation of relative amide proton exchange rates of 15 N-labelled proteins by a straightforward water selective NOESY-HSQC experiment. FEBS Lett 383:191–195

Chan DI, Vogel HJ (2010) Current understanding of fatty acid biosynthesis and the acyl carrier protein. Biochem J 430:1–19

Chen J-H, Cutting B, Bodenhausen G (2000) Measurement of radiation damping rate constants in nuclear magnetic resonance by inversion recovery and automated compensation of selective pulses. J Chem Phys 112:6511–6514

Chevelkov V, Xue Y, Rao DK, Forman-Kay JD, Skrynnikov NR (2010) 15 N H/D-SOLEXSY experiment for accurate measurement of amide solvent exchange rates: application to denatured drkN SH3. J Biomol NMR 46:227–244

Christoffersen M, Bolvig S, Tüchsen E (1996) Salt effects on the amide hydrogen exchange of bovine pancreatic trypsin inhibitor. Biochemistry 35:2309–2315

Connelly GP, Bai Y, Jeng MF, Englander SW (1993) Isotope effects in peptide group hydrogen exchange. Proteins 17:87–92

Delaglio F, Grzesiek S, Vuister GW, Zhu G, Pfeifer J, Bax A (1995) NMRpipe—a multidimensional spectral processing system based on Unix pipes. J Biomol NMR 6:277–293

Dobson CM, Lian L-Y, Redfield C, Topping KD (1986) Measurement of hydrogen exchange rates using 2D NMR spectroscopy. J Magn Reson 69:201–209

Englander SW, Kallenbach NR (1983) Hydrogen exchange and structural dynamics of proteins and nucleic-acids. Q Rev Biophys 16:521–655

Fitzkee NC, Torchia DA, Bax A (2011) Measuring rapid hydrogen exchange in the homodimeric 36 kDa HIV-1 integrase catalytic core domain. Protein Sci 20:500–512

Geen H, Freeman R (1991) Band-selective radiofrequency pulses. J Magn Reson 93:93–141

Gemmecker G, Jahnke W, Kessler H (1993) Measurement of fast proton-exchange rates in isotopically labeled compounds. J Am Chem Soc 115:11620–11621

Grzesiek S, Bax A (1993) Measurement of amide proton exchange rates and NOEs with water in 13C/15 N-enriched calcineurin B. J Biomol NMR 3:627–638

Hwang TL, Mori S, Shaka AJ, van Zijl PCM (1997) Application of phase-modulated CLEAN chemical EXchange spectroscopy (CLEANEX-PM) to detect water-protein proton exchange and intermolecular NOEs. J Am Chem Soc 119:6203–6204

Hwang TL, van Zijl PCM, Mori S (1998) Accurate quantitation of water-amide proton exchange rates using the Phase-Modulated CLEAN chemical EXchange (CLEANEX-PM) approach with a Fast-HSQC (FHSQC) detection scheme. J Biomol NMR 11: 221–226

Jeener J, Meier BH, Bachmann P, Emst RR (1979) Investigation of exchange processes by two-dimensional NMR spectroscopy. J Chem Phys 71:4546–4553

Kay LE, Keifer P, Saarinen T (1992) Pure absorption gradient enhanced heteronuclear single quantum correlation spectroscopy with improved sensitivity. J Am Chem Soc 114:10663–10665

Liepinsh E, Otting G (1995) Selective excitation of intense solvent signals in the presence of radiation damping. J Biomol NMR 5:420–426

Lim J, Rong K, Murugan E, Ho CL, Liang Z, Yang D (2011) Solution structures of the acyl carrier protein domain from the highly reducing Type I iterative polyketide synthase CalE8. Plos One 6:e20549

Lipari G, Szabo A (1982) Model-free approach to the interpretation of nuclear magnetic relaxation in macromolecules: 1. Theory and range of validity. J Am Chem Soc 104:4546–4559

Mao XA, Ye C (1997) Understanding radiation damping in a simple way. Concepts Magn Reson 9:173–187

Miao XJ, Jin-Hong Chen JH, Mao XA (1999) Selective excitation by radiation damping field for a coupled nuclear spin system. Chem Phys Lett 304:45–50

Mori S, Johnson MO, Berg JM, Vanzijl PCM (1994) Water exchange filter (wex filter) for nuclearmagnetic-resonance studies of macromolecules. J Am Chem Soc 116:11982–11984

Mori S, Berg JM, van Zijl PCM (1996a) Separation of intramolecular NOE and exchange peaks in water exchange spectroscopy using spin-echo filters. J Biomol NMR 7:77–82

Mori S, Abeygunawardana C, van Zijl PCM, Berg JM (1996b) Water exchange filter with improved sensitivity (WEX II) to study solvent-exchangeable protons. Application to the consensus zinc finger peptide CP-1. J Magn Reson B 110:96–101

Mori S, Abeygunawardana C, Berg JM, Peter CM, van Zijl PCM (1997) NMR study of rapidly exchanging backbone amide protons in staphylococcal nuclease and the correlation with structural and dynamic properties. J Am Chem Soc 119:6844–6852

Otting G, Liepinsh E, Wüthrich K (1991) Protein hydration in aqueous solution. Science 254:974–980

Parris KD, Lin L, Tam A, Mathew R, Hixon J, Stahl M, Fritz CC, Seehra J, Somers WS (2000) Crystal structures of substrate binding to Bacillus subtilis holo-(acyl carrier protein) synthase reveal a novel trimeric arrangement of molecules resulting in three active sites. Structure 8:883–895

Paterson Y, Englander SW, Roder H (1990) An antibody binding site on cytochrome c defined by hydrogen exchange and two-dimensional NMR. Science 249(4970):755–759

Spera S, Ikura M, Bax A (1991) Measurement of the exchange rates of rapidly exchanging amide protons. Application to the study of calmodulin and its complex with a myosin light chain kinase fragment. J Biomol NMR 1:155–166

Vijay-Kumar S, Charles E, Bugg CE, Cook WJ (1987) Structure of ubiquitin refined at 1.8 Å resolution. J Mol Biol 194:531–544

Wagner G, Wüthrich K (1982) Amide proton exchange and surface conformation of the basic pancreatic trypsin inhibitor in solution: studies with two-dimensional nuclear magnetic resonance. J Mol Biol 160:343–361